This is an *Accepted Manuscript*, which has been through the Royal Society of Chemistry peer review process and has been accepted for publication.

Accepted Manuscripts are published online shortly after acceptance, before technical editing, formatting and proof reading. Using this free service, authors can make their results available to the community, in citable form, before we publish the edited article. We will replace this *Accepted Manuscript* with the edited and formatted *Advance Article* as soon as it is available.

You can find more information about *Accepted Manuscripts* in the **Information for Authors**.

Journal Name

COMMUNICATION

Heterostructured ZnO/SnO$_{2-x}$ Nanoparticles for Efficient Photocatalytic Hydrogen Production

Mingyang Li, Yue Hu, Shilei Xie, Yongchao Huang, Yexiang Tong* and Xihong Lu*

Heterostructured ZnO/SnO$_{2-x}$ nanoparticles (NPs) were synthesized by a facile two-step hydrothermal process for the first time and exhibited excellent photocatalytic activity due to the increased oxygen vacancies and matched band edge alignment.

Due to the energy crisis, the development of alternative of energy calls for vigorous consideration. Photocatalytic hydrogen production from water over semiconductor oxides under solar irradiation is one of the most promising and friendly methods.[1] Various semiconductor oxides have been intensively investigated as photocatalysts for hydrogen production.[2] As an important n-type semiconductor, SnO$_2$ has attracted great attentions as photoactive material in fields of photocatalysis and solar cells due to its excellent optical properties.[3] With respect to photochemical properties, SnO$_2$ exhibits high stability, and thus it has the potential to be an ideal photocatalyst. However, few applications of SnO$_2$ have been developed into the photocatalytic hydrogen production performance, due to the quick recombination of photo-generated charge carriers and the large band gap ($E_g \approx 3.6$ eV). Therefore, suppression of the recombination of charge carriers or decreasing the large band gap is essential for improving photocatalytic hydrogen production performance.

Oxygen vacancies have been proven to play an important role in determining the physical and chemical properties of semiconductor oxides, and recent reports have shown that the presence of oxygen vacancies can effectively improve the conductivity and suppress the electron-hole recombination rate, and thus dramatically enhancing the photoactivity of oxides.[4] Energy levels of oxygen vacancies in SnO$_2$ are located below the bottom edge of the conduction band, and served as shallow donors for SnO$_2$.[2b] On the other hand, the conduction band (CB) of ZnO is negative than that of SnO$_2$, while the valence band (VB) of SnO$_2$ is positive than that of ZnO. When they combine to form heterostructures could suppress the charge recombination and enhance the photocatalytic performance.[5] We

hypothesize that the photocatalytic activity of SnO$_2$ could be significantly enhanced by introduced oxygen vacancies and incorporated with ZnO. Experimental results demonstrated that ZnO decorated oxygen-deficient SnO$_2$ (denoted as ZnO/SnO$_{2-x}$) NPs exhibited substantially higher photocatalytic activity than the stoichiometric SnO$_2$ NPs and SnO$_{2-x}$ NPs. The ZnO/SnO$_{2-x}$ NPs achieved a high hydrogen evolution rate of 182.6 μmol h^{-1} g^{-1} with good stability.
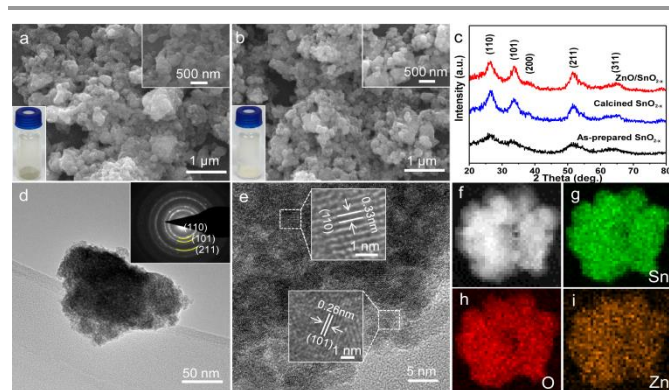

Fig. 1 (a-b) SEM and photo images of Calcined SnO$_{2-x}$ and ZnO/SnO$_{2-x}$; (c) XRD patterns of As-prepared, Calcined SnO$_{2-x}$ and ZnO/SnO$_{2-x}$; (d-e) TEM, HRTEM images and SAED pattern of ZnO/SnO$_{2-x}$ NPs; (f-i) EDS elemental maps of ZnO/SnO$_{2-x}$.

Heterostructured ZnO/SnO$_{2-x}$ NPs were synthesized by a two-step process. Firstly, yellow SnO$_{2-x}$ powders were obtained by a typical hydrothermal reaction according to previous literature (Experimental section). To improve the crystallinity, the as-prepared SnO$_{2-x}$ powders were annealed at 350 °C in N$_2$ for 3 h, and the color of powders changed from yellow to brownish (Figure 1a). Scanning electron microscopy (SEM) images reveal that the as-prepared SnO$_{2-x}$ powders were made up of NPs with a diameter of 400-500 nm (Figure S1). In order to obtain the heterostructured ZnO/SnO$_{2-x}$ NPs, the as-

prepared SnO_{2-x} powders were immersed into a 6 mM $Zn(NO_3)_2$ solution for 30 min under stirring, and then annealed in N_2 at 350 °C for 3 h. The color of the resulted powder was greyish white, and SEM studies confirm that there are no obvious morphological changes for SnO_{2-x} NPs after combined with ZnO. X-ray diffraction (XRD) spectra of as-prepared SnO_{2-x}, calcined SnO_{2-x} and ZnO/SnO_{2-x} were collected and shown in Figure 1b. All the diffraction peaks can be well indexed to rutile SnO_2 (JCPDS # 41-1445). The similar shapes of the diffraction peaks suggest that the annealing and incorporation with ZnO did not affect lattice structure and size of SnO_{2-x} (Fig. S2). No any peaks of ZnO were detected due to the small amount of ZnO. In addition, the broad diffraction peaks indicate the crystal sizes of the SnO_{2-x} and ZnO/SnO_{2-x} NPs are very small. Transmission electron microscopy (TEM) were used to further study the microstructure of ZnO/SnO_{2-x} NPs. Fig. 1d displays a typical TEM image of ZnO/SnO_{2-x} sample, indicating that the ZnO/SnO_{2-x} were composed of many NPs with a small size of 5-7 nm. Selected-area electron diffraction (SAED) analysis reveals that the ZnO/SnO_{2-x} NPs were highly crystallinity with a rutile SnO_2 structure (inset in Fig. 1d). The clear lattice fringes further confirm the high crystalline nature of ZnO/SnO_{2-x} NPs (Fig. 1e). The measured lattice fringes of 0.33 and 0.26 nm are consistent with the d-spacing of (110) and (101) planes of rutile SnO_2 (JCPDF # 41-1445). In order to further elucidate microscopic structure, scanning TEM (STEM)-EDS elemental map was also conducted, and the results are shown in Fig. 1f-i. Sn, O and Zn were uniformly distributed on the NPs, indicating the formation of ZnO and SnO_{2-x} heterostructure.
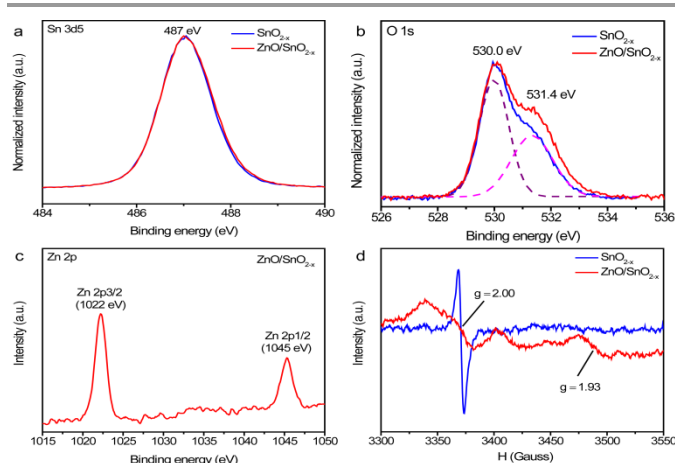

Fig.2 Normalized (a) Sn3d5 and (b) O 1s core level XPS spectra of SnO_{2-x} and ZnO/SnO_{2-x}; (c) Zn 2p core level XPS spectrum of ZnO/SnO_{2-x}; (d) EPR spectra SnO_{2-x} and ZnO/SnO_{2-x} recorded at 88 K.

X-ray photoelectron spectroscopy (XPS) was used to determine the chemical composition and surface oxidation states of SnO_{2-x} and ZnO/SnO_{2-x} samples. The Sn 3d5 peaks located at 487 eV in both samples are consistent with the values reported for Sn^{4+} (Fig. 2a), which indicates the chemical state of Sn presented in SnO_{2-x} and ZnO/SnO_{2-x} is similar. Fig. 2b compares the O 1s core level XPS spectra of SnO_{2-x} and ZnO/SnO_{2-x} samples. The peaks centered at the binding energy around 530 eV correspond to the Sn-O-Sn bonds, while the peaks centered around 531.4 eV are ascribed to oxygen vacancy or Sn-O-H bonds.[6] Significantly, the ZnO/SnO_{2-x} sample displays a much stronger peak at the higher binding energy compared to SnO_{2-x},

which indicates an increasing density of oxygen vacancy and hydroxyl groups on the surface of SnO_{2-x} after the incorporation with ZnO. Fig. 2c shown Zn 2p3 and Zn 2p1 lines at the binding energies of about 1022 and 1045 eV, which are consistent with the values recorded for ZnO.[2b] For better understanding the presence of oxygen vacancy in the lattice, we also recorded the electron paramagnetic resonance (EPR) spectra (Fig. 2d). EPR spectra of SnO_{2-x} displayed the resonance at g ≈ 2.00 with well symmetry attributed to the presence of oxygen vacancy.[7] The sharper and higher peak further confirmed there existing oxygen vacancy in the crystal lattice of SnO_{2-x} samples has higher activity. With respect to ZnO/SnO_{2-x} EPR spectrum, the as-received powders exhibited a broad signal at g ≈ 2.00 and lower symmetric signal at g ≈ 1.93. Che et al.[8] had reported the broadening line and ascribed it to the magnetic interaction occurring from collisions of oxygen with surface species. Therefore, the wave line with g ≈ 2.00 might indicate the increasing shallow defects in ZnO/SnO_{2-x}, such as oxygen vacancies, which can absorb more oxygen molecules from the atmosphere. Meanwhile, when the unpaired electron was suppressed by the conditions of ions, such as detection temperature and chemical status of adjacent ions, the signals could be broader. In this case, we also presumed the presence of ZnO on the surface which led to the broadening line. Moreover, the lower symmetrical resonance line obtained at g ≈ 1.93, which is widely reported in the literature [7b], was always present in native SnO_2. This proved that ZnO/SnO_{2-x} sample owns more stable oxygen vacancy in lattices than SnO_{2-x} sample, which is further confirmed by photoluminescence (PL) spectra (Fig. S3). The higher intensity of PL peaks of ZnO/SnO_{2-x} samples suggests it has more oxygen vacancies.[9]

To study the influence of oxygen vacancy and ZnO on the photocatalytic activity of SnO_{2-x} NPs, we have examined the rates of hydrogen production of the SnO_{2-x} and ZnO/SnO_{2-x} NPs in a 100 ml aqueous solution under light irradiation. Commercial TiO_2 (P25), ZnO NPs (Fig. S4) and stoichiometric SnO_2 NPs were also tested under the same conditions for comparison. Stoichiometric SnO_2 NPs were obtained by annealed as-prepared SnO_2 at 350 °C in air for 3 h. XRD and EPR studies confirm they are stoichiometric SnO_2 with rutile structure (Fig. S5). Fig. 3a shows the time-dependent photocatalytic hydrogen evolution of the P25, ZnO, SnO_2, SnO_{2-x}, and ZnO/SO_{2-x} samples. As expected, the ZnO/SnO_{2-x} NPs exhibited the best photocatalytic activity. The average hydrogen evolution rate of the SnO_2 NPs is only 24.4 μmol h^{-1} g^{-1}, while the SnO_{2-x} and ZnO/SnO_{2-x} NPs achieved 133.8 and 182.6 μmol h^{-1} g^{-1}, respectively. This result fully confirms that the introduction of oxygen vacancies and incorporation of ZnO can significantly improve the photocatalytic activity of SnO_2. Moreover, the average rate of the ZnO/SnO_{2-x} NPs is also faster than that of commercial P25 and ZnO NPs (118.8 and 106.8 μmol h^{-1} g^{-1}). The improved photocatalytic activity of ZnO/SnO_{2-x} NPs might be attributed to its improved light-harvesting ability and fast separation and transport of photoexcited electron-hole arising from oxygen vacancies and the matched band edge alignment of this heterostructure. On the other hand, the ZnO/SnO_{2-x} NPs have excellent stability. After three cycles, the photocatalytic activity of ZnO/SnO_{2-x} NPs has no obvious change (Fig. 3b).
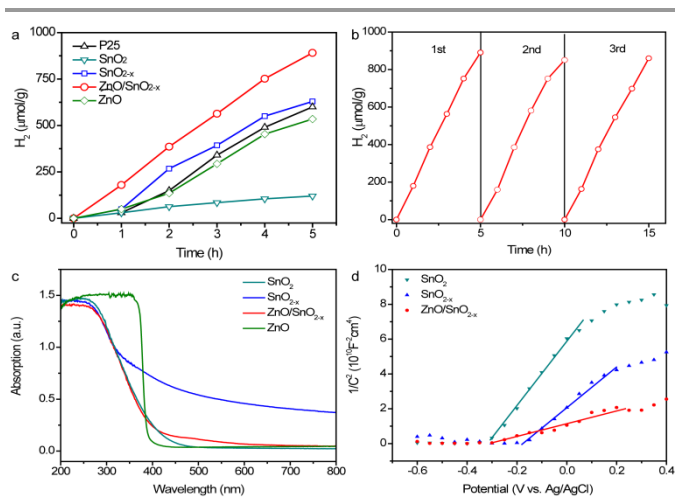
Fig.3 (a) Photocatalytic hydrogen production rate collected for P25, SnO₂, SnO₂₋ₓ, ZnO and ZnO/SnO₂₋ₓ under white light irradiation; (b) Cycling test of ZnO/SnO₂₋ₓ; (c) UV-visible spectra of SnO₂, SnO₂₋ₓ, ZnO and ZnO/SnO₂₋ₓ; (d) Mott-Schottky plots of SnO₂, SnO₂₋ₓ, and ZnO/SnO₂₋ₓ.

In order to elucidate the enhanced photocatalytic activity of ZnO/SnO₂₋ₓ NPs, UV-visible absorption spectra for samples were shown in Figure 3c. ZnO NPs has the best UV light-harvesting ability but poorer photolytic activity than SnO₂₋ₓ and ZnO/SnO₂₋ₓ samples. The SnO₂, SnO₂₋ₓ and ZnO/SnO₂₋ₓ samples exhibited a similar absorption edge at about 330 nm, which consistent with the band-gap of SnO₂ (3.6 eV). In comparison to the SnO₂, the relative higher absorption of SnO₂₋ₓ and ZnO/SnO₂₋ₓ samples in the wavelength range between 400 and 700 nm suggests that they can absorb visible light. Given that, we also studied their photocatalytic performance under visible light irradiation ($\lambda \geq$ 420 nm). However, no hydrogen evolution was observed for both the SnO₂₋ₓ and ZnO/SnO₂₋ₓ NPs, which indicates that the enhanced photocatalytic activity of SnO₂₋ₓ and ZnO/SnO₂₋ₓ is not due to their improved visible light absorption. Electrochemical impedance measurements were performed to investigate their electrical properties (Experimental section). As display in Fig. 3d, all the samples exhibited positive slopes in the Mott-Schottky plots, showing their n-type semiconductor feature. Carrier denor density of semiconductor can be calculated to be 6.0×10^{19}, 9.9×10^{19} and 2.9×10^{20} cm⁻³, respectively. As expected, the carrier density of SnO₂ increased significantly after introduced oxygen vacancies and could further increase by incorporated with ZnO as a result of their matched band edge alignment. On the other hand, the surface areas of SnO₂, SnO₂₋ₓ and ZnO/SnO₂₋ₓ calculated by the Brunauer-Emmett-Teller (BET) method are similar with 23~25 m² g⁻¹ (Experimental section). Therefore, based on the results above, it is believed that the increased oxygen vacancies and matched band edge alignment are the main reasons for the enhanced photocatalytic performance of the ZnO/SnO₂₋ₓ NPs.

Conclusions

In summary, we have demonstrated that the photocatalytic activity of SnO₂ NPs could be substantially enhanced via introduction of oxygen vacancy and incorporation with ZnO. Due to the dramatically increased donor density, ZnO/SnO₂₋ₓ NPs yield a remarkable hydrogen evolution rate of 182.6 µmol h⁻¹ g⁻¹, which is much higher than those of SnO₂ and SnO₂₋ₓ NPs. Moreover, the ZnO/SnO₂₋ₓ NPs have a good photostability. These findings open up new opportunities to obtain high-performance SnO₂-based photoanode for water splitting.

Notes and references

KLGHEI of Environment and Energy Chemistry, MOE of the Key Laboratory of Bioinorganic and Synthetic Chemistry, School of Chemistry and Chemical Engineering, Sun Yat-Sen University, Guangzhou 510275, China. E-mail: chedhx@mail.sysu.edu.cn; luxh6@mail.sysu.edu.cn Fax: +86 20 84112245; Tel: +86 20 84110071
†Electronic Supplementary Information (ESI) available: [Experimental details, SEM of As-prepared SnO₂₋ₓ, TEM of Calcined SnO₂₋ₓ, Room temperature PL spectra of SnO₂₋ₓ and ZnO/SnO₂₋ₓ NPs, SEM of ZnO and XRD and EPR spectra of SnO₂, BET]. See DOI: 10.1039/c000000x/

1. (a)G. Wang, Y. Ling, X. Lu, H. Wang, F. Qian, Y. Tong and Y. Li, *Energy. Environ. Sci.*, 2012, **5**, 8215-8219; (b)J. Zhou, G. Tian, Y. Chen, X. Meng, Y. Shi, X. Cao, K. Pan and H. Fu, *Chem. Commun.*, 2013, **49**, 2237-2239.
2. (a)A. Fujishima and K. Honda, *Nature*, 1972, **238**, 37-38; (b)X. Lu, G. Wang, S. Xie, J. Shi, W. Li, Y. Tong and Y. Li, *Chem. Commun.*, 2012, **48**, 7717-7719; (c)Y. Ling, G. Wang, J. Reddy, C. Wang, J. Z. Zhang and Y. Li, *Angew Chem Int Ed Engl*, 2012, **51**, 4074-4079.
3. (a)W. W. Wang, Y. J. Zhu and L. X. Yang, *Adv. Funct. Mater.*, 2007, **17**, 59-64; (b)N. Li, K. Du, G. Liu, Y. Xie, G. Zhou, J. Zhu, F. Li and H.-M. Cheng, *J. Mater. Chem. A*, 2013, **1**, 1536.
4. (a)X. Lu, G. Wang, T. Zhai, M. Yu, J. Gan, Y. Tong and Y. Li, *Nano Lett.*, 2012, **12**, 1690-1696; (b)J. Gan, X. Lu, J. Wu, S. Xie, T. Zhai, M. Yu, Z. Zhang, Y. Mao, S. C. I. Wang, Y. Shen and Y. Tong, *Sci. Rep.*, 2013, **3**.
5. (a)M. T. Uddin, Y. Nicolas, C. Olivier, T. Toupance, L. Servant, M. M. Muller, H. J. Kleebe, J. Ziegler and W. Jaegermann, *Inorg. Chem.*, 2012, **51**, 7764-7773; (b)Z. H. Wen, G. Wang, W. Lu, Q. Wang, Q. Zhang and J. H. Li, *Cryst. Growth. Des.*, 2007, **7**, 1722-1725.
6. C. H. Liang, Y. Shimizu, T. Sasaki and N. Koshizaki, *J. Phys. Chem. B*, 2003, **107**, 9220-9225.
7. (a)N. Chiodini, F. Meinardi, F. Morazzoni, J. Padovani, A. Paleari, R. Scotti and G. Spinolo, *J. Mater. Chem.*, 2001, **11**, 926-929; (b)A. Gurlo, *Chemphyschem : a European journal of chemical physics and physical chemistry*, 2006, **7**, 2041-2052.
8. M. Che and A. Tench, *Adv. Catal.*, 1983, **31**, 77.
9. E. J. H. Lee, C. Ribeiro, T. R. Giraldi, E. Longo, E. R. Leite and J. A. Varela, *Appl. Phys. Lett.*, 2004, 84, 1745.